Structure-based design of a selective heparanase inhibitor as an antimetastatic agent

Keisuke Ishida,[1,2] Go Hirai,[3] Koji Murakami,[2] Takayuki Teruya,[1,4] Siro Simizu,[1] Mikiko Sodeoka,[3] and Hiroyuki Osada[1,4]

[1]Antibiotics Laboratory, RIKEN Discovery Research Institute, Saitama, Japan; [2]Hanno Discovery Center, Taiho Pharmaceutical Co., Ltd., Saitama, Japan; [3]Institute of Multidisciplinary Research for Advanced Materials, Tohoku University, Miyagi, Japan; and [4]Graduate School of Science and Engineering, Saitama University, Saitama, Japan

Abstract

Heparanase is an endo-β-D-glucuronidase that degrades heparan sulfate glycosaminoglycans in the extracellular matrix and the basement membrane and is well known to be involved in tumor cell invasion and angiogenesis. We have focused on heparanase as a target for antitumor agents, especially antimetastatic agents. (*R*)-3-hexadecanoyl-5-hydroxymethyltetronic acid (RK-682) was found to display an inhibitory activity against heparanase in our screening of natural sources. Because RK-682 has been reported to show inhibitory activities against several enzymes, we have tried to develop selective heparanase inhibitors using the method of rational drug design. Based on the structure of the heparanase/RK-682 complex, we speculated that selective inhibitory activity against heparanase could be acquired by arylalkylation, namely, by benzylation of the 4-position of RK-682. Among the rationally designed 4-alkyl-RK-682 derivatives, 4-benzyl-RK-682 has been found to possess a selective inhibitory activity for heparanase (IC_{50} for heparanase, 17 μmol/L; IC_{50} for other enzymes, >100 μmol/L). 4-Benzyl-RK-682 also inhibited the invasion and migration of human fibrosarcoma HT1080 cells (IC_{50} for invasion, 1.5 μmol/L; IC_{50} for migration, 3.0 μmol/L). On the other hand, RK-682 had no inhibitory effect on the invasion and migration of HT1080 cells at doses of up to 100 μmol/L. [Mol Cancer Ther 2004;3(9):1069–77]

Received 12/26/03; revised 5/18/04; accepted 7/6/04.

Grant support: Ministry of Education, Science, Sports, Culture and Technology of Japan and the Chemical Biology Project (RIKEN).

The costs of publication of this article were defrayed in part by the payment of page charges. This article must therefore be hereby marked advertisement in accordance with 18 U.S.C. Section 1734 solely to indicate this fact.

Requests for reprints: Hiroyuki Osada, Antibiotics Laboratory, RIKEN Discovery Research Institute, 2-1 Hirosawa, Wako, Saitama 351-0198, Japan. Phone: 81-48-467-9541; Fax: 81-48-462-4669.
E-mail: hisyo@riken.jp

Introduction

Heparanase is an endo-β-D-glucuronidase that degrades heparan sulfate glycosaminoglycans (1). Human heparanase cDNA encodes the latent enzyme, which consists of 543 amino acid residues, and becomes the active enzyme of 50 kDa after being processed twice at the amino terminus (2, 3). Because only one heparanase cDNA sequence coding functional enzyme has been identified to date, heparanase has been considered a major enzyme that degrades heparan sulfate glycosaminoglycans in mammalian tissues (4–7). High-level expression of heparanase enzyme has been found in highly invasive normal and malignant cells, such as activated immune cells, lymphoma, melanoma, and carcinoma cells (2, 8–11), as well as in human head and neck tumors (12). Further, heparanase expression has been correlated with the metastatic property of tumor cells (2, 10, 11, 13) and experimental metastasis in an animal model was shown to be reduced by treatment with heparanase inhibitors (14, 15). It has also been shown that patients with a high-level expression of heparanase mRNA tend to have a shorter postoperative survival term (16, 17). Heparanase also enhances angiogenesis by the release of growth factors, such as basic fibroblast growth factor and vascular endothelial growth factor, which are sequestered by heparan sulfate glycosaminoglycans in the extracellular matrix (10, 18–20). From these results, heparanase has been assumed to be a promising target for antitumor agents, especially antimetastatic agents.

Most of the heparanase inhibitors that have been reported are sulfated oligosaccharide derivatives that resemble the substrate of heparan sulfate glycosaminoglycans (15, 21–23). We have established a heparan sulfate degradation assay system to develop novel heparanase inhibitors that are not sulfated oligosaccharide derivatives and have used it to screen 10,000 microbial broths of actinomycetes, fungi, and bacteria (24). As a result, (*R*)-3-hexadecanoyl-5-hydroxymethyltetronic acid (RK-682; Fig. 1A), which we had purified previously as a potent inhibitor of tyrosine phosphatase (25), was found to possess a potent inhibitory activity for heparanase (24). The IC_{50} value of RK-682 for heparanase was 17 μmol/L; this is a fairly low value compared with, for example, the IC_{50} of suramin, a known heparanase inhibitor, which is 46 μmol/L (26).

RK-682 has already been shown to have several inhibitory activities, including phospholipase A2 inhibition (IC_{50}, 16 μmol/L; ref. 27), HIV-1 protease inhibition (IC_{50}, 84 μmol/L; refs. 28, 29), and protein tyrosine phosphatase inhibition (IC_{50} of CD45, 54 μmol/L; IC_{50} of vaccinia H1-related phosphatase, 2.0 μmol/L; ref. 25). In the present study, we therefore attempted to develop a heparanase selective inhibitor based on rational drug design using RK-682 as a lead structure and investigated the antitumor activity.

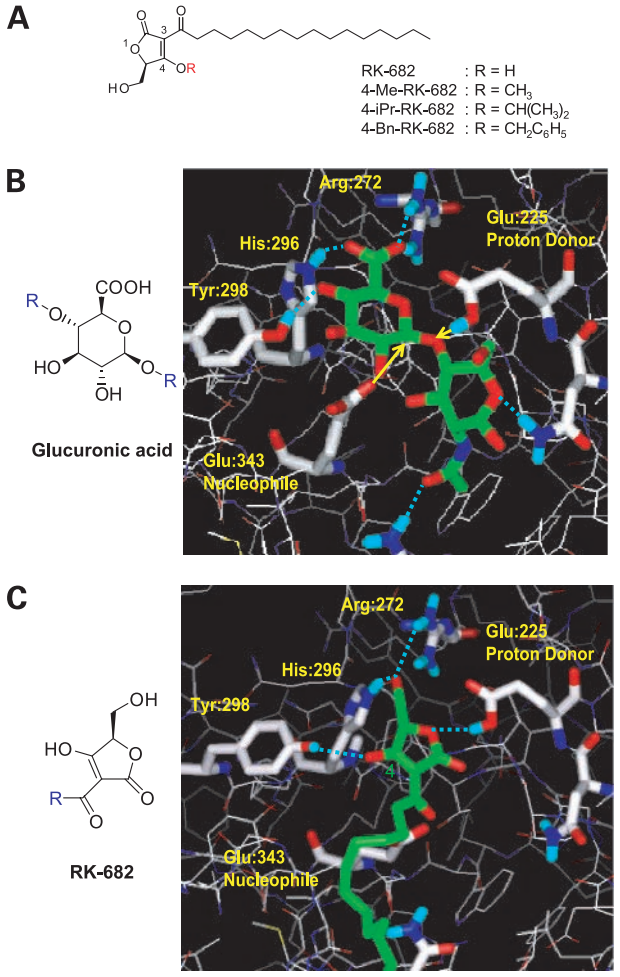

Figure 1. Speculated molecular basis of the interaction between heparanase and ligands. **A,** structures of RK-682 and its 4-alkyl derivatives. **B,** interaction between the active site of heparanase and an heparan sulfate disaccharide, GlcA-GlcNAc. **C,** interaction between the active site of heparanase and RK-682. Heparan sulfate, RK-682, active-site Glu residues, and the amino acid residues that interacted with ligands are in *boldface type*. Atoms in heparan sulfate and RK-682 are in *green* (carbon), *red* (oxygen), and *blue* (nitrogen). Atoms in heparanase are in *white* (carbon), *red* (oxygen), *blue* (nitrogen), and *light blue* (hydrogen). *Yellow arrows,* enzyme reaction of Glu^{225} (proton donor) and Glu^{343} (nucleophile). *Blue dashed lines*, hydrogen bonds.

Materials and Methods

Homology Modeling of Heparanase and Construction of the Heparanase/RK-682 Complex

The amino acid sequence alignment of human heparanase and 1,4-β-xylanase from *Penicillium simplicissimum* (EC 3.2.1.8) was carried out manually using the Homology module of the Discover/InsightII programs (Accelrys, Inc., San Diego, CA). Structurally conserved regions were defined by referring to the results of database searches and site-directed mutagenesis by Hulett et al. (30). Structure construction and molecular dynamics calculations were carried out by the Biopolymer and Discover3 modules of Discover/InsightII program (Accelrys) using the X-ray structure of 1,4-β-xylanase (Protein Data Bank entry 1BG4) as a template (31).

Synthesis of 4-Methyl-RK-682

4-Methyl-RK-682 (4-Me-RK-682) was prepared as described previously (32). RK-682 was treated with diazomethane in diethyl ether at 23°C for 20 minutes.

Synthesis of 4-Isopropyl-RK-682

1,2,3-Triisopropyl-isourea was prepared as described previously (33). A solution of RK-682 (30.0 mg, 81.4 μmol) and 1,2,3-triisopropyl-isourea (30.3 mg, 162.8 μmol) in 0.5 mL dry tetrahydrofuran was stirred under reflux for 18 hours. After cooling to room temperature, the solution was concentrated. The residue was purified by silica gel column chromatography (hexane/ethyl acetate, 5:1) and preparative thin-layer chromatography on silica gel (hexane/ethyl acetate, 1:1) to give 4-isopropyl-RK-682 (4-iPr-RK-682, 6.8 mg, 20%): $[\alpha]_D^{24}$ = 5.76 (c = 0.20, $CHCl_3$); Fourier transformation-IR (film) 3,440, 2,917, 2,850, 1,722, 1,672, 1,603, 1,466, 1,409, 1,317, 1,097, 1,048 cm^{-1}; ^1H nuclear magnetic resonance (400 MHz, $CDCl_3$) δ 5.38 (1H, septet, J = 5.6 Hz), 4.70 (1H, triplet, J = 3.2 Hz), 4.05 (1H, multiplet), 3.85 (1H, multiplet), 3.00 (1H, double triplet, J = 18.0, 7.8 Hz), 2.94 (1H, double triplet, J = 18.0, 7.8 Hz), 1.87 (1H, broad), 1.57 (2H, multiplet), 1.25 (22H, multiplet), 0.87 (5H, multiplet); ^{13}C nuclear magnetic resonance (100 MHz, $CDCl_3$) δ 197.7, 177.2, 105.3, 79.6, 78.7, 61.5, 42.5, 31.9, 29.9, 29.68, 29.66, 29.62, 29.52, 29.48, 29.4, 29.2, 27.4, 23.8, 22.7, 22.1, 21.8, 14.1; matrix-associated laser desorption/ionization time of flight mass spectroscopy (positive ion, α-cyano-4-hydroxycynnamic acid) calculated for $C_{24}H_{42}O_5Na$: $(M + Na)^+$ 433.293; found 433.235.

Synthesis of 4-Benzyl-RK-682

2-Benzyl-1,3-dicyclohexyl-isourea was prepared as described previously (33). A solution of RK-682 (30.0 mg, 81.4 μmol) and 2-benzyl-1,3-dicyclohexyl-isourea (51.2 mg, 162.8 μmol) in 0.5 mL dry tetrahydrofuran was stirred under reflux for 24 hours. After cooling to room temperature, the solution was concentrated. The residue was purified by silica gel column chromatography (hexane/ethyl acetate, 5:1) and preparative thin-layer chromatography on silica gel (hexane/ethyl acetate, 1:1) to give 4-benzyl-RK-682 (4-Bn-RK-682, 20.1 mg, 54%): $[\alpha]_D^{24} = -0.25$ (c = 0.75, $CHCl_3$); Fourier transformation-IR (film) 3,422, 2,918, 2,850, 1,766, 1,607, 1,433, 1,368, 1,329, 1,232, 1,075 cm^{-1}; ^1H nuclear magnetic resonance (400 MHz, $CDCl_3$) δ 7.41-7.30 (5H, multiplet), 5.50 (1H, doublet, J = 12.0 Hz), 5.34 (1H, doublet, J = 12.0 Hz), 4.78 (1H, triplet, J = 3.2 Hz), 4.08 (1H, broad multiplet), 3.90 (1H, broad multiplet), 2.87 (1H, double triplet, J = 17.8, 7.6 Hz), 2.78 (1H, double triplet, J = 17.8, 7.6 Hz), 2.04 (1H, broad), 1.51 (2H, multiplet), 1.25 (22H, multiplet), 0.86 (5H, multiplet); ^{13}C nuclear magnetic resonance (100 MHz, $CDCl_3$) δ 197.8, 177.5, 170.3, 134.2, 129.1, 128.8, 128.0, 106.9, 78.7, 77.4, 61.2, 42.4, 39.0, 31.9, 29.67, 29.66, 29.65, 29.62, 29.5, 29.45, 29.3, 29.1, 28.0, 27.4, 23.6, 22.69, 22.65, 14.1; matrix-associated

laser desorption/ionization time of flight mass spectroscopy (positive ion, α-cyano-4-hydroxycynnamic acid) calculated for $C_{28}H_{42}O_5Na$: $(M + Na)^+$ 481.293; found 481.224.

Cell Culture

The heparanase-overexpressing stable clone of HepG2 human hepatocellular carcinoma cell line, HepG2-HP, was cultured in DMEM supplemented with 10% FCS and 400 μg/mL G418 (geneticin, Life Technologies, Grand Island, NY; ref. 34). HepG2 cells, human fibrosarcoma HT1080 cells, and murine B16BL6 melanoma cells were grown in DMEM supplemented with 10% FCS. All cell lines were incubated at 37°C in a humidified atmosphere of 5% CO_2/95% air.

Heparanase Inhibition Assay

Heparan sulfate was purchased from Seikagaku Corp. (Tokyo, Japan). A mixture of 90 μL HepG2-HP cell lysate (2.0 mg/mL protein) and 10 μL heparan sulfate solution (10 mg/mL in PBS, pH 6.2) with or without compound solution was incubated for 24 hours at 37°C. After adding the 20 μL heparan sulfate sampling solution [glycerol 8 mL, bromophenol blue (5 mg/mL in H_2O) 5 mL, H_2O 19 mL], the reaction mixture (10 μL) was subjected to SDS-PAGE (20%). Electrophoresed gel was soaked in H_2O for 2 hours to remove SDS. The gel was stained with 0.5% Alcian Blue 8GX for 3 hours and destained with a 1:2:7 mixture of acetic acid/ethanol/water for 12 hours (35). The volumes of the bands were measured using a MD Scanning Imager equipped with MD ImageQuant Software version 3.22 (Molecular Dynamics, Inc., Sunnyvale, CA) for quantification.

Vaccinia H1-Related Phosphatase Inhibition Assay

Assay condition was described previously (32). The mixture of *p*-nitrophenyl phosphate (10 mmol/L) and vaccinia H1-related phosphatase (0.25 μmol/L), which was overexpressed in *Escherichia coli* and purified, with or without a compound was incubated at 37°C for 30 minutes and the absorbance was measured at 405 nm.

Glycosidase Inhibition Assay

Glycosidase activities were assessed using the method described previously (36, 37). All enzymes and substrates were purchased from Sigma Chemical Co. (St. Louis, MO). α-Glucosidase (yeast) was incubated at 37°C for 30 minutes in citrate phosphate buffer (0.025 mol/L, pH 6.3) using *p*-nitrophenyl α-D-glucopyranoside as a substrate. β-Glucosidase (almond) or β-glucuronidase (bovine liver) was assayed at 37°C for 30 minutes in acetate buffer (0.1 mol/L, pH 5.0) using *p*-nitrophenyl β-D-glucopyranoside or phenolphthalein mono-β-D-glucuronic acid as substrates, respectively.

Invasion and Migration Assay

In vitro invasion and migration activities were assessed using the method of Albini et al. (38) For the invasion assay, the BD BioCoat Matrigel Invasion Chambers (Becton Dickinson Labware, Bedford, MA) were used. On the other hand, no Matrigel-coated cell culture inserts (Becton Dickinson Labware) were used for the migration assay. The chambers were placed on 24-well plates. Tumor cell suspension (0.5 mL, 5×10^4 cells/mL) in DMEM (0% FCS) was added to the upper layer and 0.75 mL DMEM (10% FCS) was added to the lower layer. After adhesion for 1 hour, compounds or vehicle were added to the upper and lower layers, and for the HepG2 cells, human hepatocyte growth factor/scatter factor (R&D Systems, Inc., Minneapolis, MN) was also used as additive. After incubation for 20 hours at 37°C, the tumor cells and Matrigel on the upper surface of the membrane were completely removed by wiping the membrane with cotton swabs. The cells on the lower surface of the membrane were fixed with methanol and stained with 0.5% crystal violet. The cells from various regions of the membrane were counted and the percentage inhibition was calculated by the following equation: % inhibition = 100 − (cell number of the compound-treated experiment) / (cell number of the vehicle-treated experiment) × 100.

Wound Healing Assay

Wound healing assay was carried out using the method described previously (39). HT1080 cells (5×10^5 cells/well in six-well plate) were incubated in dishes for 24 hours. An artificial wound was carefully created using plastic tip to scratch on the subconfluent cell monolayer. The medium was changed and the cells were treated with chemicals for 20 hours and were taken photographs.

Cell Viability Assay

The viability of tumor cells was measured by a trypan blue exclusion assay. Cell suspension (500 μL, 2×10^5 cells/mL) was added to the wells of a 24-well plate (1×10^5 cells/well) and incubated at 37°C for 12 hours. The cells were treated with either compounds or vehicle (DMSO) at 37°C for 48 hours. After trypsination (100 μL), 400 μL medium was added and 20 μL trypan blue solution [0.05% in PBS (−)] was added to the cell suspension (80 μL). After 10 minutes at room temperature, cell number was measured using a hemocytometer.

The viability of tumor cells was also measured by a 2-(2-methoxy-4-nitrophenyl)-3-(4-nitrophenyl)-5-(2,4-disulfophenyl)-2H tetrazolium, monosodium salt (Nacalai Tesque, Kyoto, Japan) assay (40). Cell suspension (100 μL, 1×10^5 cells/mL) was added to the wells of a 96-well plate (1×10^4 cells/well) and incubated at 37°C for 12 hours. The cells were treated with either compounds or vehicle (DMSO) at 37°C for 48 hours. 2-(2-Methoxy-4-nitrophenyl)-3-(4-nitrophenyl)-5-(2,4-disulfophenyl)-2H tetrazolium, monosodium salt solution (10 μL, 5 mmol/L) was added to the wells and the mixtures were incubated at 37°C for 2 hours. The absorbance was measured at 450 nm. The relative cell number was calculated as a percentage by the following equation: % relative cell number = $(A - B) / (C - B) \times 100$, where A is the absorbance of the sample solution, B is the absorbance of the negative control, and C is the absorbance of the positive control.

Adhesion Assay

Tumor cells were incubated with vehicle or compounds for 48 hours. The tumor cell suspension in DMEM (0% FCS) was added to human fibronectin cellware 35 mm dishes, collagen IV cellware 35 mm dishes, laminin cellware

35 mm dishes, or poly-D-lysine cellware 35 mm dishes (Becton Dickinson Labware). The plate was incubated at 37°C for 1 hour. After washing the plate with PBS, the adherent cells were fixed with glutaraldehyde and stained with crystal violet. Cells from various regions of the wells were counted and the percentage inhibition was calculated by the following equation: % inhibition = 100 − (cell number of a chemical-treated experiment) / (cell number of the vehicle-treated experiment) × 100.

Results

Construction of the Heparanase/RK-682 Complex Model

The results of database searches and site-directed mutagenesis suggested that mammalian heparanase is related to the members of glycosyl hydrolase families 10, 39, and 51. Homology modeling of heparanase was done using the X-ray structure of 1,4-β-xylanase from *P. simplicissimum* (Protein Data Bank entry 1BG4), which is a member of the glycosyl hydrolase family 10, as a template. The heparan sulfate dimer, GlcA-GlcNAc (where GlcA and GlcNAc represent D-glucuronic acid and *N*-acetyl-D-glucosamine, respectively), was manually located on the active site of heparanase and the complex model was constructed using molecular mechanics and molecular dynamics calculations in consideration of the mechanism of enzymatic glycoside hydrolysis (41, 42). Based on the results, it was reasonable to assume that the protonation of the exocyclic oxygen in the glycosidic bond by Glu^{225} (proton donor) and the interaction between Glu^{343} (catalytic nucleophile) and the anomeric carbon atom of GlcA occurred in this heparanase/heparan sulfate model and that hydrogen bonds contributed to the stabilization of the complex structure (Fig. 1B). We assumed that the chemical structure of RK-682 mimics that of GlcA. Thus, RK-682 was located at the position of GlcA in consideration of their structural similarity and the complex model of heparanase/RK-682 was constructed by the molecular mechanics/molecular dynamics calculations. Hydrogen bonds between Arg^{272} and 5-OH of RK-682, between His^{296} and 5-OH of RK-682, between Tyr^{298} and 4-OH of RK-682, and between Glu^{225} and 1-O of RK-682 stabilized the heparanase/RK-682 complex, just as they have been shown to stabilize the heparanase/heparan sulfate complex (Fig. 1C). The alkyl side chain of RK-682 was located along the cleft structure of heparanase, which consists of hydrophobic amino acids such as valine, leucine, and phenylalanine.

Working Hypothesis for Development of a Heparanase Selective Inhibitor

In the heparanase/RK-682 complex model, the 4-OH group of RK-682 looked toward the amino acids of His^{296} and Tyr^{298} (Figs. 1C and 2A) and we therefore speculated that the interaction between heparanase and RK-682 derivatives was more stabilized by the arylalkylation, as in the benzylation of the 4-OH group of RK-682 (Fig. 2B). It has been reported that 3-acyltetronic acids are extremely acidic; for example, the p*K*a value of 3-acetyltetronic acid is 0.8 (43). The acidic 3-acyltetronic acid structure of RK-682 acting as a phosphate mimic is very important to interact with protein tyrosine phosphatases and dual-specificity phosphatases (Fig. 2C). If the 4-OH group of RK-682 was blocked by alkylation, RK-682 was neutralized and decreased the binding strength to protein tyrosine phosphatases/dual-specificity phosphatases (Fig. 2D). Based on these data, we hypothesized that 4-Bn-RK-682 selectively inhibits heparanase.

Synthesis of RK-682 Derivatives

We have carried out the chemical modification of RK-682 to obtain a specific inhibitor of heparanase. 4-Me-RK-682, 4-iPr-RK-682, and 4-Bn-RK-682 were prepared from RK-682 by the treatment of diazomethane, 1,2,3-triisopropyl-isourea, and 2-benzyl-1,3-dicyclohexyl-isourea, respectively (Fig. 1A).

Inhibitory Activities of RK-682 Derivatives against Heparanase, Vaccinia H1-Related Phosphatase, and Glycosidases

The inhibitory activities of RK-682 derivatives against heparanase, vaccinia H1-related phosphatase, and glycosidases are shown in Fig. 3 and Table 1. RK-682 and 4-Bn-RK-682 inhibited heparanase equally (the IC_{50} values of both compounds were 17 μmol/L; Fig. 3A; Table 1). 4-Me-RK-682 and 4-iPr-RK-682 scarcely showed heparanase inhibition (the IC_{50} values of both compounds were >100 μmol/L; Fig. 3A; Table 1). RK-682 showed a potent inhibitory activity against vaccinia H1-related phosphatase (the

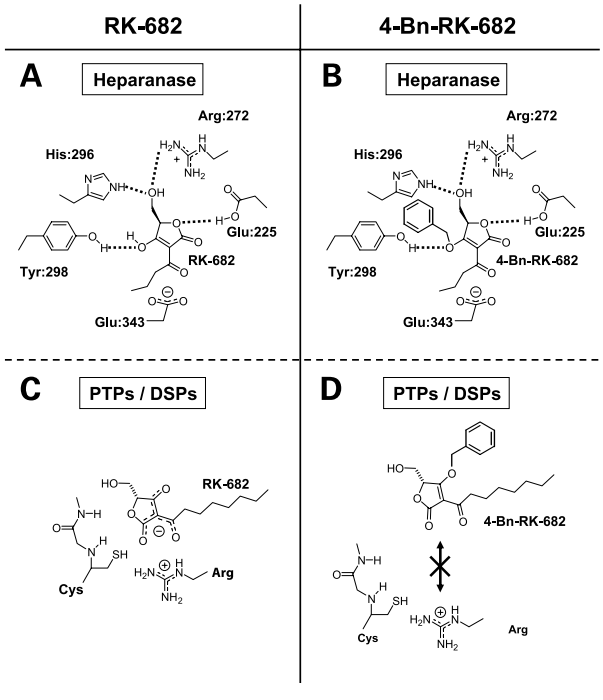

Figure 2. Working hypothesis for the development of a heparanase selective inhibitor. Schematic diagrams of the interaction between heparanase and RK-682 (**A**) or 4-Bn-RK-682 (**B**) and between protein tyrosine phosphatases/dual-specificity phosphatases (*PTPs/DSPs*) and RK-682 (**C**) or 4-Bn-RK-682 (**D**). *Dashed lines,* hydrogen bonds.

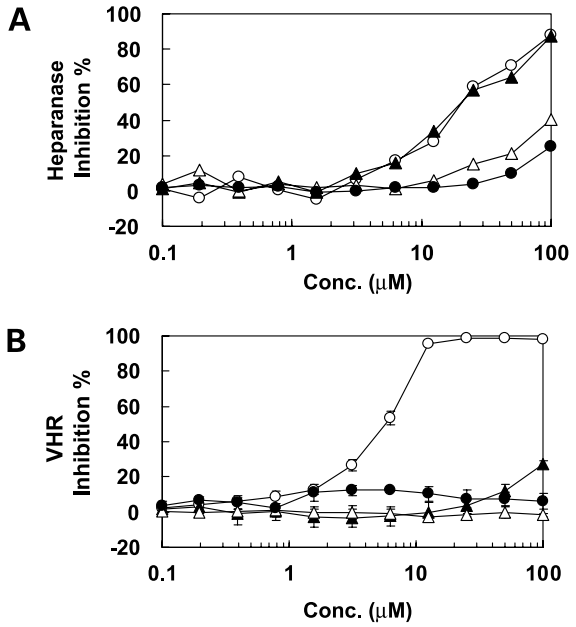

Figure 3. Inhibitory activities of RK-682 derivatives against heparanase and vaccinia H1-related phosphatase (*VHR*). **A,** dose-response curves of heparanase inhibition by treatment with RK-682 derivatives. *Points,* mean of two experiments. **B,** dose-response curves of vaccinia H1-related phosphatase inhibition by treatment with RK-682 derivatives. *Points,* mean of three experiments; *bars,* SD. ○, RK-682; ●, 4-Me-RK-682; △, 4-iPr-RK-682; ▲, 4-Bn-RK-682.

IC_{50} value was 6 μmol/L; Fig. 3B; Table 1). The inhibitory activities of 4-alkylated derivatives of RK-682 against vaccinia H1-related phosphatase were considerably reduced (the IC_{50} values of these compounds were >100 μmol/L; Fig. 3B; Table 1). The selectivity (taken as the IC_{50} value of vaccinia H1-related phosphatase divided by that of heparanase) of RK-682 was 0.4, whereas that of 4-Bn-RK-682 was >6. The heparanase selectivity of 4-Bn-RK-682 was >15-fold that of RK-682. Effects of RK-682 derivatives against other glycosidases (α-glucosidase, β-glucosidase, and β-glucuronidase) were also assayed. All compounds had no inhibitory activities against all these enzymes at a dose of 100 μmol/L (Table 1).

Effects of 4-Bn-RK-682 against Migration and Invasion

4-Bn-RK-682 remarkably inhibited both migration and invasion of HT1080 cells, whereas RK-682 showed no inhibitory activities against migration and invasion at 100 μmol/L (Fig. 4Aa). The IC_{50} values of 4-Bn-RK-682 against the migration and invasion of HT1080 cells were 3.0 and 1.5 μmol/L, respectively. Whereas the invasion of HT1080 was not inhibited by treatment with vehicle (Fig. 4Ab) or 100 μmol/L RK-682 (Fig. 4Ac), 4-Bn-RK-682 at a concentration of only 10 μmol/L completely inhibited the invasion of HT1080 cells (Fig. 4Ad). In the HepG2 cell line that is heparanase deficient, 4-Bn-RK-682 did not exert any anti-invasive effect (Fig. 4B). There was no difference in the inhibition of invasion and migration of HT1080 cells by RK-682 and 4-Bn-RK-682 in the presence of heparan sulfate (Fig. 4C). Tumor cell migration was also studied using an *in vitro* wound healing assay (Fig. 4D). Confluent HT1080 cells were scratched (Fig. 4Da) and treated with chemicals for 20 hours. After the treatment with vehicle (DMSO) or RK-682 (100 μmol/L), HT1080 cells migrated and covered a great area of the scratch (Fig. 4Db and Dc). On the other hand, 10 μmol/L 4-Bn-RK-682 significantly inhibited the migration of HT1080 cells (Fig. 4Dd).

Effects of 4-Bn-RK-682 against Growth and Adhesion

As results of trypan blue exclusion assay (Fig. 5Aa) and 2-(2-methoxy-4-nitrophenyl)-3-(4-nitrophenyl)-5-(2,4-disulfophenyl)-2H tetrazolium, monosodium salt assay (Fig. 5Ab), neither RK-682 nor 4-Bn-RK-682 showed cytotoxicity and cell growth inhibition at a dose of <100 μmol/L. It is very interesting that the treatment of 4-Bn-RK-682 makes HT1080 cells adhesive (Fig. 5B). Adherent cell number was increased by the treatment of 4-Bn-RK-682 against all of the tested adhesion molecules (i.e., fibronectin, collagen IV, laminin, poly-D-lysine, and plastic). The increase was most significant against collagen IV.

Discussion

RK-682 was known to inhibit the dual-specificity protein phosphatase vaccinia H1-related phosphatase (25). 4-Bn-RK-682, which was rationally designed based on the docking model with heparanase, inhibited heparanase (IC_{50}, 17 μmol/L) without inhibiting vaccinia H1-related

Table 1. Inhibitory activities of RK-682 derivatives against heparanase, vaccinia H1-related phosphatase, and glycosidases

Compounds	IC_{50} (μmol/L)				
	Heparanase	Vaccinia H1-Related Phosphatase	α-Glucosidase	β-Glucosidase	β-Glucuronidase
RK-682	17	6	>100	>100	>100
4-Me-RK-682	>100	>100	>100	>100	>100
4-iPr-RK-682	>100	>100	>100	>100	>100
4-Bn-RK-682	17	>100	>100	>100	>100

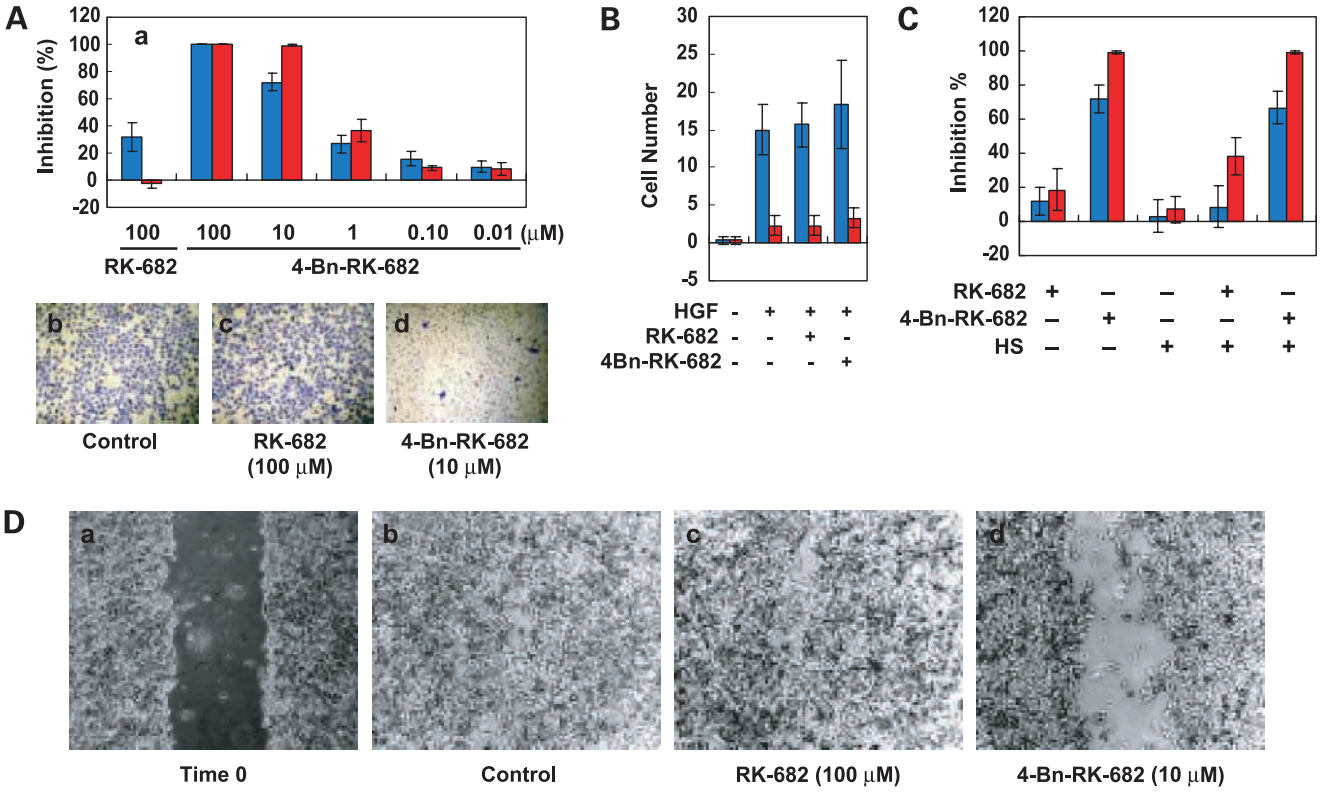

Figure 4. Effects of 4-Bn-RK-682 against migration and invasion. **A,** *a,* inhibition of migration and invasion of HT1080 cells by RK-682 and 4-Bn-RK-682. *Columns,* mean of three experiments; *bars,* SD. *Blue columns,* migration (without Matrigel); *red columns,* invasion (with Matrigel). Descriptions for graphs are the same and applied to **B** and **C**. *b–d,* images of the invaded HT1080 cells treated with vehicle (*Control*, *b*), RK-682 (100 μmol/L, *c*), or 4-Bn-RK-682 (10 μmol/L, *d*) for 20 hours on the 8 μm pore membrane. **B,** inhibition of migration and invasion of HepG2 cells by RK-682 and 4-Bn-RK-682. **C,** inhibition of migration and invasion of HT1080 cells by RK-682 and 4-Bn-RK-682 with or without heparan sulfate (*HS*). **D,** migration analysis by *in vitro* wound healing assay. After incubation of HT1080 cells (5×10^5 cells/well of six-well plate) for 24 hours, an artificial ''wound'' was created using a plastic tip (*a*). Cells were treated with vehicle (*Control*, *b*), RK-682 (100 μmol/L, *c*), or 4-Bn-RK-682 (10 μmol/L, *d*) for 20 hours.

phosphatase at dose of up to 100 μmol/L. The level of heparanase inhibition by 4-Bn-RK-682 was comparable or more potent than that by the other small molecular heparanase inhibitors reported to date. The small molecular heparanase inhibitors have been reported by other groups as follows. The IC_{50} values of suramin, Evans blue, and trypan blue against murine B16BL6 melanoma heparanase were 46, 320, and 320 μmol/L, respectively (26). Trachyspic acid purified from the culture broth of *Talaromyces trachyspermus* SANK 12191 inhibited murine B16BL6 melanoma heparanase at IC_{50} value of 36 μmol/L (44). A-72363 A-1, A-2, and C (the diastereomers of siastatin B, a neuraminidase inhibitor) were purified from the culture filtrate of *Streptomyces nobilis* SANK 60192 in the screening for heparanase inhibitors. A-72363 C inhibited heparanase from B16BL6 cells (IC_{50}, 12 μmol/L) and β-glucuronidase from bovine liver (IC_{50}, 1.6 μmol/L; refs. 45, 46). A transition state mimic of glycosidase, D-galacturonic acid–type *gem*-diamine 1-*N*-iminosugar, also potently inhibited heparanase from human melanoma A375M cells (IC_{50}, 1.0 μmol/L) and β-glucuronidase from bovine liver (IC_{50}, 0.065 μmol/L; ref. 47).

In either cases, A-72363 C and D-galacturonic acid–type *gem*-diamine 1-*N*-iminosugar have potent inhibitory activity for heparanase than 4-Bn-RK-682, but both compounds are iminosugar derivatives having strong inhibitory activity for β-glucuronidase rather than heparanase (45–47). 4-Bn-RK-682, however, is not a sugar mimic and does not show inhibitory activity for other glycosidases (Table 1).

4-Bn-RK-682 inhibited the invasion and migration of human fibrosarcoma HT1080 cells at low concentration (the IC_{50} values against the invasion and migration were 1.5 and 3.0 μmol/L, respectively), whereas the compounds did not show any inhibitory activities against migration and invasion of HepG2 cells (Fig. 4A and B). We have reported previously that heparanase mRNA and protein expression levels were hardly detectable in HepG2 cells (12). These results indicate that antimigrative and anti-invasive effects of 4-Bn-RK-682 are related with the heparanase inhibition by the compound. Additive heparan sulfate did not affect the inhibitory activities of 4-Bn-RK-682 against migration and invasion (Fig. 4C). This result suggests that 4-Bn-RK-682 does not interact with heparan sulfate and the drug may bind to heparanase rather than substrate heparan sulfate.

Heparan sulfate is one of the main components of extracellular matrix (Matrigel) and is ubiquitously existent at the cell surface. Therefore, the accessibility of additive heparan sulfate to the Matrigel and the cell surface is not well because of the electrostatic repulsion of negative charge. Heparanase is existent at the cell surface and in the medium. Additive heparan sulfate is possible to inhibit heparanase in the medium but not at the cell surface and did not inhibit the migration and invasion of HT1080 cells (Fig. 4C). From these aspects, it is suggested that heparanase at the cell surface but not in the medium is important for the migration and invasion of HT1080 cells. It is reported by other groups that addition of heparanase stimulated phosphoinositide 3-kinase–dependent endothelial cell migration and invasion (48).

4-Bn-RK-682 showed neither cytotoxicity nor cell growth inhibition at a dose of <100 μmol/L (Fig. 5Aa and Ab). These results indicate that the remarkable inhibition of cell invasion and migration was caused by neither cytotoxicity nor cell growth inhibition. Heparan sulfate glycosaminoglycans act as physical barriers in the extracellular matrix and the basement membrane and tumor cells harness heparanase to destroy heparan sulfate glycosaminoglycans for invasion. Therefore, in the invasion assay using Matrigel as a barrier, it is reasonable that a selective heparanase inhibitor, 4-Bn-RK-682, inhibited the invasion of HT1080 cells. But why 4-Bn-RK-682 also inhibited the migration of HT1080 cells in the experiment using no Matrigel is unclear. One answer is that 4-Bn-RK-682 inhibited the migration of HT1080 cells by increasing adherence of the cells (Fig. 5B). It was reported previously that a heparanase inhibitor inhibited the migration and invasion of HT1080 cells by increasing the adherence of the cells (31). Furthermore, heparanase has been known to involve in tumor migration by the degradation of cell surface heparan sulfate glycosaminoglycans of heparan sulfate proteoglycans (e.g., syndecans), which is a key mechanism of cell spreading and migration. For example, syndecan-4 is located at sites of cell-matrix adhesion (49), and regulates cell spreading and migration, in cooperation with integrins (50, 51). Thus, the present findings indicating that heparanase inhibition by 4-Bn-RK-682 results in inhibition of the invasion and migration of HT1080 cells are consistent with the previous reports. The invasion and migration of HT1080 cells were also inhibited by the antiheparanase antibody treatment (31). This result supports that there is a correlation between the heparanase inhibition and the invasion/migration inhibition.

We successfully produced a heparanase selective inhibitor by the benzylation at the 4-position of RK-682 according to a working hypothesis guided by the heparanase/

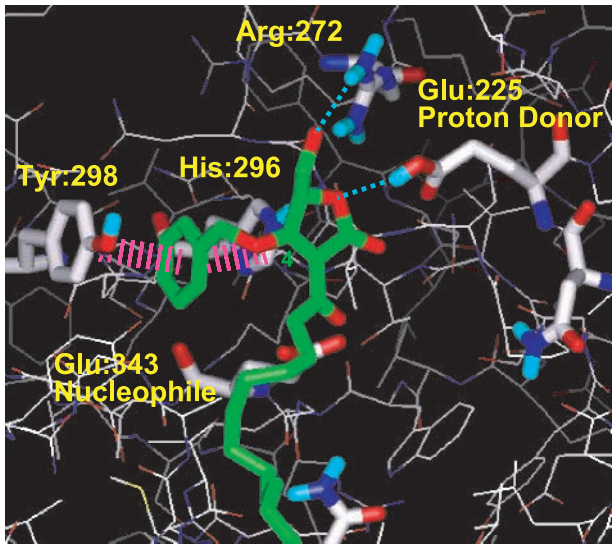

Figure 6. Speculated molecular basis of the interaction between heparanase and 4-Bn-RK-682. 4-Bn-RK-682, active-site Glu residues, and the amino acid residues that interacted with RK-682 are in *boldface type*. Atoms in 4-Bn-RK-682 are in *green* (carbon) and *red* (oxygen). Atoms in heparanase are in *white* (carbon), *red* (oxygen), *blue* (nitrogen), and *light blue* (hydrogen). *Blue dashed lines,* hydrogen bonds. *Pink hatched lines,* π-π stacking interactions.

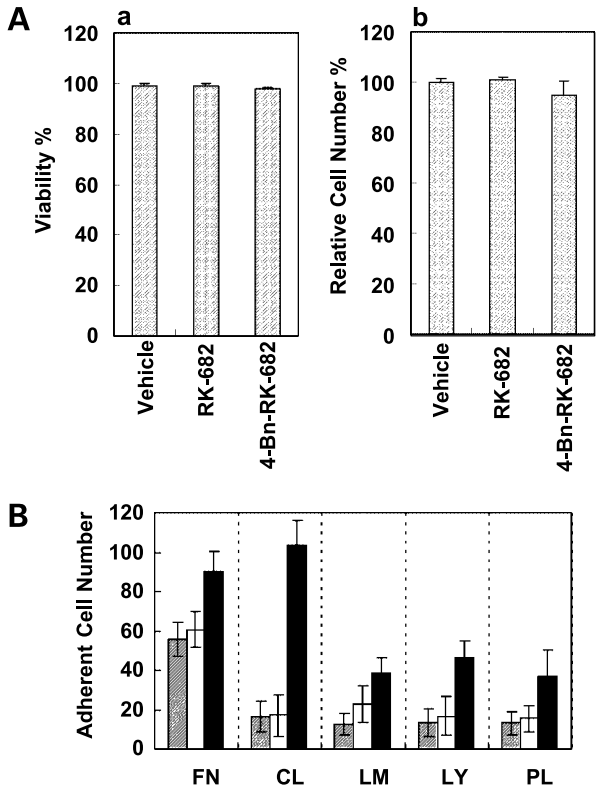

Figure 5. Effects of 4-Bn-RK-682 against growth and adhesion. **A,** cell viability assay. *a,* trypan blue exclusion assay; *b,* 2-(2-methoxy-4-nitrophenyl)-3-(4-nitrophenyl)-5-(2,4-disulfophenyl)-2H tetrazolium, monosodium salt assay. *Columns,* mean of three experiments; *bars,* SD. HT1080 cells were treated with vehicle, RK-682 (100 μmol/L), or 4-Bn-RK-682 (100 μmol/L) for 48 hours. **B,** increase of adherence of HT1080 cells by 4-Bn-RK-682. *Columns,* mean of three experiments; *bars,* SD. *Gray*, *white*, and *black columns,* treatment of vehicle, RK-682 (100 μmol/L), or 4-Bn-RK-682 (10 μmol/L) for 48 hours, respectively. *FN,* fibronectin; *CL,* collagen IV; *LM,* laminin; *LY,* poly-D-lysine; *PL,* plastic.

RK-682 docking model. In addition, we attempted to assess the biological activity of the compound for which α/β-naphthylmethyl group was substituted at the 4-position, but this biological evaluation was hard to execute because of the weak water solubility of the compounds. The molecular mechanics/molecular dynamics calculation led the speculated interaction model of heparanase/4-Bn-RK-682 (Fig. 6). Two hydrogen bonds (between Arg^{272} and 5-OH of 4-Bn-RK-682 and between Glu^{225} and 1-O of the drug) stabilize the complex. The benzyl group at 4-position of 4-Bn-RK-682 contributes to stabilize the complex by the π-π stacking with Tyr^{298} and His^{296}, instead of the hydrogen bonds between His^{296} and 5-OH of RK-682, and between Tyr^{298} and 4-OH of RK-682 in the heparanase/RK-682 complex model (Fig. 1C).

This is the first report of a heparanase inhibitor that has noncharged character. Negatively charged RK-682 inhibited not only heparanase activity but also other enzyme activities. In sulfated oligosaccharides, an oligosaccharide chain length and a degree of sulfation are critical to inhibit angiogenesis and heparanase activity (14). These inhibitory activities might be exhibited by not only heparanase inhibition but also interfering with the formation of a ternary complex, which consists of heparan sulfate binding growth factor, heparan sulfate, and growth factor receptor (20, 52). In iminosugar derivatives, other glycosidases, especially β-glucuronidase, were inhibited instead of heparanase (46, 47). Negative charge–dependent interaction between a heparan sulfate binding growth factor and heparan sulfate may not be interfered by noncharged 4-Bn-RK-682. Therefore, 4-Bn-RK-682 could be assumed as a pure heparanase inhibitor different from other inhibitors described previously.

Whereas the IC_{50} values of RK-682 and 4-Bn-RK-682 against heparanase were equal, RK-682 showed no inhibitory activities for cell-based assays (migration and invasion). This result may be caused by the difference of accessibility to the cell membrane. The neutral character of 4-Bn-RK-682 was effective against cellular effects as compared with RK-682 possessing negative charge. These results indicate that 4-Bn-RK-682 could be assumed not only as a bioprobe for decipherment heparanase function but also as a promising antimetastatic agent.

References

1. Bame KJ. Heparanases: endoglycosidases that degrade heparan sulfate proteoglycans. Glycobiology 2001;11:91 – 8R.

2. Parish CR, Freeman C, Hulett MD. Heparanase: a key enzyme involved in cell invasion. Biochim Biophys Acta 2001;1471:M99 – 108.

3. Fairbanks MB, Mildner AM, Leone JW, et al. Processing of the human heparanase precursor and evidence that the active enzyme is a heterodimer. J Biol Chem 1999;274:29587 – 90.

4. Toyoshima M, Nakajima M. Human heparanase. Purification, characterization, cloning, and expression. J Biol Chem 1999;274:24153 – 60.

5. Vlodavsky I, Friedmann Y, Elkin M, et al. Mammalian heparanase: gene cloning, expression and function in tumor progression and metastasis. Nat Med 1999;5:793 – 802.

6. Hulett MD, Freeman C, Hamdorf BJ, Baker RT, Harris MJ, Parish CR. Cloning of mammalian heparanase, an important enzyme in tumor invasion and metastasis. Nat Med 1999;5:803 – 9.

7. Kussie PH, Hulmes JD, Ludwig DL, et al. Cloning and functional expression of a human heparanase gene. Biochem Biophys Res Commun 1999; 261:183 – 7.

8. Dempsey LA, Brunn GJ, Platt JL. Heparanase, a potential regulator of cell-matrix interactions. Trends Biochem Sci 2000;25:349 – 51.

9. Vlodavsky I, Eldor A, Haimovitz-Friedman A, et al. Expression of heparanase by platelets and circulating cells of the immune system: possible involvement in diapedesis and extravasation. Invasion Metastasis 1992;12:112 – 27.

10. Vlodavsky I, Friedmann Y. Molecular properties and involvement of heparanase in cancer metastasis and angiogenesis. J Clin Invest 2001; 108:341 – 7.

11. Nakajima M, Irimura T, Nicolson GL. Heparanases and tumor metastasis. J Cell Biochem 1988;36:157 – 67.

12. Simizu S, Ishida K, Wierzba MK, Sato TA, Osada H. Expression of heparanase in human tumor cell lines and human head and neck tumors. Cancer Lett 2003;193:83 – 9.

13. Nakajima M, Irimura T, Di Ferrante D, Di Ferrante N, Nicolson GL. Heparan sulfate degradation: relation to tumor invasive and metastatic properties of mouse B16 melanoma sublines. Science 1983;220:611 – 3.

14. Vlodavsky I, Mohsen M, Lider O, et al. Inhibition of tumor metastasis by heparanase inhibiting species of heparin. Invasion Metastasis 1994;14: 290 – 302.

15. Parish CR, Freeman C, Brown KJ, Francis DJ, Cowden WB. Identification of sulfated oligosaccharide-based inhibitors of tumor growth and metastasis using novel *in vitro* assays for angiogenesis and heparanase activity. Cancer Res 1999;59:3433 – 41.

16. Gohji K, Hirano H, Okamoto M, et al. Expression of three extracellular matrix degradative enzymes in bladder cancer. Int J Cancer 2001;95: 295 – 301.

17. Koliopanos A, Friess H, Kleeff J, et al. Heparanase expression in primary and metastatic pancreatic cancer. Cancer Res 2001;61:4655 – 9.

18. Elkin M, Ilan N, Ishai-Michaeli R, et al. Heparanase as mediator of angiogenesis: mode of action. FASEB J 2001;15:1661 – 3.

19. Goldshmidt O, Zcharia E, Abramovitch R, et al. Cell surface expression and secretion of heparanase markedly promote tumor angiogenesis and metastasis. Proc Natl Acad Sci U S A 2002;99:10031 – 6.

20. Nugent MA, Iozzo RV. Fibroblast growth factor-2. Int J Biochem Cell Biol 2000;32:115 – 20.

21. Irimura T, Nakajima M, Nicolson GL. Chemically modified heparins as inhibitors of heparan sulfate specific endo-β-glucuronidase (heparanase) of metastatic melanoma cells. Biochemistry 1986;25:5322 – 8.

22. Bar-Ner M, Eldor A, Wasserman L, et al. Inhibition of heparanase-mediated degradation of extracellular matrix heparan sulfate by non-anticoagulant heparin species. Blood 1987;70:551 – 7.

23. Saiki I, Murata J, Nakajima M, Tokura S, Azuma I. Inhibition by sulfated chitin derivatives of invasion through extracellular matrix and enzymatic degradation by metastatic melanoma cells. Cancer Res 1990;50:3631 – 7.

24. Ishida K, Teruya T, Simizu S, Osada H. Exploitation of heparanase inhibitors from microbial metabolites using an efficient visual screening system. J Antibiot 2004;57:136 – 42.

25. Hamaguchi T, Sudo T, Osada H. RK-682, a potent inhibitor of tyrosine phosphatase, arrested the mammalian cell cycle progression at G_1 phase. FEBS Lett 1995;372:54 – 8.

26. Nakajima M, DeChavigny A, Johnson CE, Hamada J, Stein CA, Nicolson GL. Suramin. A potent inhibitor of melanoma heparanase and invasion. J Biol Chem 1991;266:9661 – 6.

27. Shinagawa S, Muroi M, Itoh T, Tobita T. Tetronic acid derivatives, its manufacturing methods and uses. Jpn Kokai Tokkyo Koho 1993;JP 05-43568:1 – 26.

28. Roggo BE, Petersen F, Delmendo R, Jenny HB, Peter HH, Roesel J. 3-Alkanoyl-5-hydroxymethyl tetronic acid homologues and resistomycin: new inhibitors of HIV-1 protease. I. Fermentation, isolation and biological activity. J Antibiot (Tokyo) 1994;47:136 – 42.

29. Roggo BE, Hug P, Moss S, Raschdorf F, Peter HH. 3-Alkanoyl-5-hydroxymethyl tetronic acid homologues: new inhibitors of HIV-1 protease. II. Structure determination. J Antibiot (Tokyo) 1994;47:143 – 7.

30. Hulett MD, Hornby JR, Ohms SJ, et al. Identification of active-site residues of the pro-metastatic endoglycosidase heparanase. Biochemistry 2000;39:15659 – 67.

31. Ishida K, Wierzba MK, Teruya T, Simizu S, Osada H. Novel heparan

sulfate mimetic compounds as antitumor agents. Chem Biol 2004;11: 367–77.

32. Sodeoka M, Sampe R, Kojima S, et al. Synthesis of a tetronic acid library focused on inhibitors of tyrosine and dual-specificity protein phosphatases and its evaluation regarding VHR and cdc25B inhibition. J Med Chem 2001;44:3216–22.

33. Mathias LJ. Esterification and alkylation reactions employing isoureas. Synthesis 1979:561–76.

34. Simizu S, Ishida K, Wierzba MK, Osada H. Secretion of heparanase protein is regulated by glycosylation in human tumor cell lines. J Biol Chem 2004;279:2697–703.

35. De Vouge MW, Yamazaki A, Bennett SA, et al. Immunoselection of GRP94/endoplasmin from a KNRK cell-specific λ gt11 library using antibodies directed against a putative heparanase amino-terminal peptide. Int J Cancer 1994;56:286–94.

36. Ichikawa Y, Igarashi Y, Ichikawa M, Suhara Y. 1-*N*-iminosugars: potent and selective inhibitors of β-glycosidases. J Am Chem Soc 1998; 120:3007–18.

37. Guo W, Hiratake J, Ogawa K, Yamamoto M, Ma SJ, Sakata K. β-D-glycosylamidines: potent, selective, and easily accessible 1-glycosidase inhibitors. Bioorg Med Chem Lett 2001;11:467–70.

38. Albini A, Iwamoto Y, Kleinman HK, et al. A rapid *in vitro* assay for quantitating the invasive potential of tumor cells. Cancer Res 1987;47: 3239–45.

39. Nakae K, Yoshimoto Y, Sawa T, et al. Migrastatin, a new inhibitor of tumor cell migration from *Streptomyces* sp. MK929-43F1. Taxonomy, fermentation, isolation and biological activities. J Antibiot (Tokyo) 2000; 53:1130–6.

40. Isobe I, Michikawa M, Yanagisawa K. Enhancement of MTT, a tetrazolium salt, exocytosis by amyloid β-protein and chloroquine in cultured rat astrocytes. Neurosci Lett 1999;266:129–32.

41. Zechel DL, Withers SG. Glycosidase mechanisms: anatomy of a finely tuned catalyst. Acc Chem Res 2000;33:11–8.

42. Lillelund VH, Jensen HH, Liang X, Bols M. Recent developments of transition-state analogue glycosidase inhibitors of non-natural product origin. Chem Rev 2002;102:515–53.

43. Yamaguchi T, Saito K, Tsujimoto T, Yuki H. NMR spectroscopic studies on the tautomerism in tenuazonic acid analogs. J Heterocyclic Chem 1976;13:533–7.

44. Shiozawa H, Takahashi M, Takatsu T, et al. Trachyspic acid, a new metabolite produced by Talaromyces trachyspermus, that inhibits tumor cell heparanase: taxonomy of the producing strain, fermentation, isolation, structural elucidation, and biological activity. J Antibiot (Tokyo) 1995;48: 357–62.

45. Takatsu T, Takahashi M, Kawase Y, et al. A-72363 A-1, A-2 and C, novel heparanase inhibitors from *Streptomyces nobilis* SANK 60192. I. Taxonomy of producing organism, fermentation, isolation and structure elucidation. J Antibiot (Tokyo) 1996;49:54–60.

46. Kawase Y, Takahashi M, Takatsu T, Arai M, Nakajima M, Tanzawa K. A-72363 A-1, A-2, and C, novel heparanase inhibitors from *Streptomyces nobilis* SANK 60192. II. Biological activities. J Antibiot (Tokyo) 1996;49: 61–4.

47. Nishimura Y, Shitara E, Adachi H, et al. Flexible synthesis and biological activity of uronic acid-type gem-diamine 1-*N*-iminosugars: a new family of glycosidase inhibitors. J Org Chem 2000;65:2–11.

48. Gingis-Velitski S, Zetser A, Flugelman MY, Vlodavsky I, Ilan N. Heparanase induces endothelial cell migration via protein kinase B/Akt activation. J Biol Chem 2004;279:23536–41.

49. Woods A, Couchman JR. Syndecan 4 heparan sulfate proteoglycan is a selectively enriched and widespread focal adhesion component. Mol Biol Cell 1994;5:183–92.

50. Wilcox-Adelman SA, Denhez F, Goetinck PF. Syndecan-4 modulates focal adhesion kinase phosphorylation. J Biol Chem 2002;277:32970–7.

51. Thodeti CK, Albrechtsen R, Grauslund M, et al. ADAM12/syndecan-4 signaling promotes β1 integrin-dependent cell spreading through protein kinase Cα and RhoA. J Biol Chem 2003;278:9576–84.

52. Vlodavsky I, Bar-Shavit R, Ishai-Michaeli R, Bashkin P, Fuks Z. Extracellular sequestration and release of fibroblast growth factor: a regulatory mechanism? Trends Biochem Sci 1991;16:268–71.